Integrating a MRI scanner with a 6 MV radiotherapy accelerator: dose deposition in a transverse magnetic field

INSTITUTE OF PHYSICS PUBLISHING PHYSICS IN MEDICINE AND BIOLOGY

Phys. Med. Biol. **49** (2004) 4109–4118 PII: S0031-9155(04)80001-0

Integrating a MRI scanner with a 6 MV radiotherapy accelerator: dose deposition in a transverse magnetic field

B W Raaymakers[1], **A J E Raaijmakers**[1], **A N T J Kotte**[1], **D Jette**[2,3] **and J J W Lagendijk**[1]

[1] Department of Radiotherapy, University Medical Center Utrecht, Heidelberglaan 100, 3584 CX, Utrecht, The Netherlands
[2] The Lawrence H Lanzl Institute of Medical Physics, PO Box 30760, Seattle, WA 98103-0760, USA
[3] Department of Medical Physics, Rush-Presbyterian-St Luke's Medical Center, Chicago, IL 60612, USA

E-mail: B.W.Raaymakers@radth.med.uu.nl

Received 28 April 2004
Published 20 August 2004
Online at stacks.iop.org/PMB/49/4109
doi:10.1088/0031-9155/49/17/019

Abstract

Integrating magnetic resonance imaging (MRI) functionality with a radiotherapy accelerator can facilitate on-line, soft-tissue based, position verification. A technical feasibility study, in collaboration with Elekta Oncology Systems and Philips Medical Systems, led to the preliminary design specifications of a MRI accelerator. Basically the design is a 6 MV accelerator rotating around a 1.5 T MRI system. Several technical issues and the clinical rational are currently under investigation. The aim of this paper is to determine the impact of the transverse 1.5 T magnetic field on the dose deposition. Monte Carlo simulations were used to calculate the dose deposition kernel in the presence of 1.5 T. This kernel in turn was used to determine the dose deposition for larger fields. Also simulations and measurements were done in the presence of 1.1 T. The pencil beam dose deposition is asymmetric. For larger fields the asymmetry persists but decreases. For the latter the distance to dose maximum is reduced by approximately 5 mm, the penumbra is increased by approximately 1 mm, and the 50% isodose line is shifted approximately 1 mm. The dose deposition in the presence of 1.5 T is affected, but the effect can be taken into account in a conventional treatment planning procedure. The impact of the altered dose deposition for clinical IMRT treatments is the topic of further research.

1. Introduction

In clinical practice, position uncertainty is dealt with by applying margins around the volume to be irradiated (International Commission on Radiation Units and Measurements (ICRU) 1999, Van Herk *et al* 2000, Stroom and Heijmen 2002). The goal of position verification is decreasing these margins, which in turn can lead to sparing of organs at risk and dose escalation. Finally this can converge to full-image-guided radiotherapy (Ling *et al* 2000). Various techniques are currently under investigation or already in clinical use to improve the position verification. For instance, transmission images of the MV-treatment beam are used and although these yield poor soft-tissue contrast they are still very suitable for positioning using the bony structure (Gilhuijs *et al* 1996) or implanted fiducial markers (Nederveen *et al* 2001). The contrast can be increased by using additional diagnostic x-ray tubes; this can be done two dimensionally, i.e. taking a single transmission image (Drake *et al* 2000), or three dimensionally by using multiple x-ray tubes and cameras (Shirato *et al* 2000).

Alternatives include the use of pre-treatment ultrasound imaging (Serago *et al* 2002), the integration of (cone-beam) CT functionality with the accelerator (Jaffray *et al* 2002) or the tomotherapy system (Mackie *et al* 1993, Ruchala *et al* 1999). The CT options yield great detail on the bony structure or implanted markers, but x-ray based soft-tissue contrast is inherently limited (Groh *et al* 2002).

The full-image-guided radiotherapy we aim for includes on-line, soft-tissue based, position verification by integrating magnetic resonance imaging (MRI) functionality with a radiotherapy accelerator (Lagendijk *et al* 2002, Raaymakers *et al* 2004). This enables direct visualization of the tumour and the surrounding structures, ultimately allowing on-line optimization of the treatment plan.

In our department we have conducted a study into the technical feasibility of such an integrated system. An artistic impression of what the system can look like is shown in figure 1. Basically the design is a conventional 1.5 T MRI system with a small, single energy (6 MV) accelerator rotating around it. In collaboration with Philips Medical Systems, Hamburg, Germany, it was found that the active magnetic shielding system of a standard system can be modified in order to magnetically decouple the accelerator and the MRI system. This requires no compromise to the magnetic field homogeneity and no additional construction complexity. The consequence of this design is the beam transmission through the MRI system. Transmission through the MRI system results in beam attenuation, scatter and field heterogeneity. Also in collaboration with Philips Medical Systems, the creation of radiation portals in the MRI system was investigated, i.e. minimizing the amount of material in the beam's eye view. Preliminary investigations show that the beam quality after transmission is acceptable. Most important was the conclusion that the integration is technically feasible.

The focus of this paper is another technical topic: the dose deposition in a 1.5 T magnetic field. Obviously the 6 MV photon beam travels unhampered in a magnetic field, however, the actual dose deposition in tissue is the result of an avalanche of secondary electrons (Khan 1994). The trajectory of these electrons is affected by the presence of a magnetic field and can be calculated using Monte Carlo simulations (Jette 2000a). The induced curvature depends on the electron energy and the magnetic field strength. Actually, given three-dimensionally controlled, high strength magnetic fields, this effect can be used to modify and optimize electron or photon beam dose distributions (Bielajew 1993, Nardi and Barnea 1999, Reiffel *et al* 2000, Jette 2000b).

The aim of this study is to investigate the impact of a 1.5 T magnetic field on the dose deposition for the specific case of our proposed integrated MRI accelerator, i.e. an axial 1.5 T

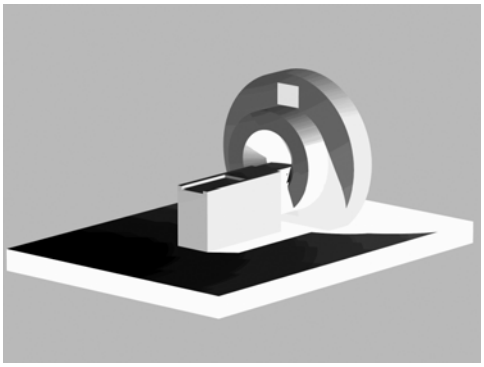

Figure 1. Artistic impression of an integrated MRI accelerator.

magnetic field perpendicular to the 6 MV photon beam. The aim is to determine the impact and significance of the magnetic field on the dose deposition.

Monte Carlo simulations will be used to determine the dose deposition kernel with and without the presence of a 1.5 T magnetic field. Also the impact on larger radiation fields, 1×1 and $5 \times 5\,\mathrm{cm}^2$, will be studied. For this study the freely available (http://geant4.web.cern.ch/geant4/) GEANT4 (Agostinelli *et al* 2003) Monte Carlo code was used, a package to simulate the passage of particles through matter. Arbitrary geometries and EM fields can be included, and a large set of particles comes with it. The package offers physics processes ranging from 250 eV up to 1 TeV. It is developed by the CERN, Switzerland, within an international collaboration of over 100 scientists and was initially developed for high energy physics applications. There is a low energy extension, which is validated specifically for medical physics purposes (Carrier *et al* 2004). Simple geometries were simulated for both photon and electron irradiation and compared with codes widely used in medical physics, i.e. MCNP (Briesmeister 1997), EGS4 (Nelson *et al* 1985) and EGSnrc (Kawrakow 2000). The mutual differences for heterogeneous media were smaller than 5% and the difference with measurements was smaller than 4%. The literature on experimental validation with the incorporation of a magnetic field has only been reported for EGS4 and did not show fair correspondence between calculation and experiment (Litzenberg *et al* 2001). While it is not the goal of this paper to validate the inclusion of magnetic fields in Monte Carlo calculations, we included experimental data for this specific set-up.

2. Methods

2.1. Monte Carlo simulations of the dose deposition kernel in a 1.5 T field

The GEANT4 Monte Carlo code was used to characterize the dose deposition kernel of a 6 MV photon pencil beam in a 1.5 T magnetic field. The realistic energy spectrum of the 6 MV photon beam of our clinical accelerator, Elekta SL_i 20, was used (Van der Zee and Welleweerd 1999). The energy spectrum was determined using BEAM (Rogers *et al* 1995), an extension on the EGS4 code (Nelson *et al* 1985) to facilitate the modelling of radiotherapy treatment units.

Geometrically, a photon pencil beam incidents the water phantom perpendicularly at the $Y = 0$ plane; at this plane also the half-space with the magnetic field of 1.5 T starts, see also figure 2. The magnetic field is directed along the Z-axis, so the expected asymmetry is in the

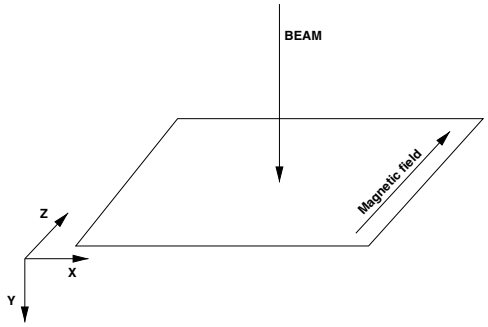

Figure 2. Schematic drawing of the set-up as used in the Monte Carlo simulations.

direction of the X-axis. The scoring region was $5 \times 5\,\mathrm{cm}^2$ for the XZ plane and 10 cm along the Y-axis, i.e. 10 cm is the maximal depth. The scoring voxels are $1 \times 1 \times 1\,\mathrm{mm}^3$.

The pencil beam dose deposition was calculated using 10 million events. By convolving the pencil beam dose deposition (with and without the presence of a magnetic field) with an arbitrary field shape, the dose distribution of larger radiation fields can be determined for a homogeneous phantom. This is done for both a 1×1 and a $5 \times 5\,\mathrm{cm}^2$ field and for both 1.5 and 1.1 T. For the pencil beam in a 1.1 T magnetic field, the volume of the magnetic field is limited to 4 cm long (that is along the Y-axis), 2 cm in the Z direction, and 3 cm in the X direction; this is in correspondence with the volume available for measurements, see also section 2.2.

Note that this way of determining the dose deposition for finite field sizes will not lead to perfect quantitative correspondence between measurements and simulations. When using the convolution with the pencil beam kernel, the penumbra will be determined merely by the phantom scatter and the magnetic field; it neglects the impact of diaphragm blocks, divergence of the beam, finite source size and beam contamination. It is beyond the scope of this paper to incorporate these detailed specifications of the measurement set-up in the Monte Carlo simulations. We are mainly interested in the impact of the magnetic field on the dose deposition, which can still be investigated since the correct energy spectrum is used.

2.2. Measuring the dose distribution of a 1 × 1 cm² field in a 1.1 T field

The dose distribution of a $1 \times 1\,\mathrm{cm}^2$ field in the presence of a 1.1 T magnetic field was measured using film dosimetry, with ready pack EDR2 films, Eastman Kodak Company, Rochester, NY, USA. The set-up was similar to the simulations for the pencil beam kernel as shown in figure 2. The magnetic field was produced by a bending magnet taken from an old Elekta SL75/20 accelerator, from which the pole shoes were adapted. The rectangular volume between the magnetic poles was 4 cm long (that is along the Y-axis), 2 cm in the Z direction and 3 cm in the X direction.

A split, water equivalent phantom was used with the film positioned in the middle of the phantom, tightly filling the space between the pole shoes. The film was positioned in the XY plane and irradiation was done with the incident beam tilted 2° along the X-axis. The latter is done to prevent over response of the film (Suchowerska *et al* 2001). Using this set-up both the depth–dose curve and the penumbra in the X direction were measured, both with and without the presence of the magnetic field.

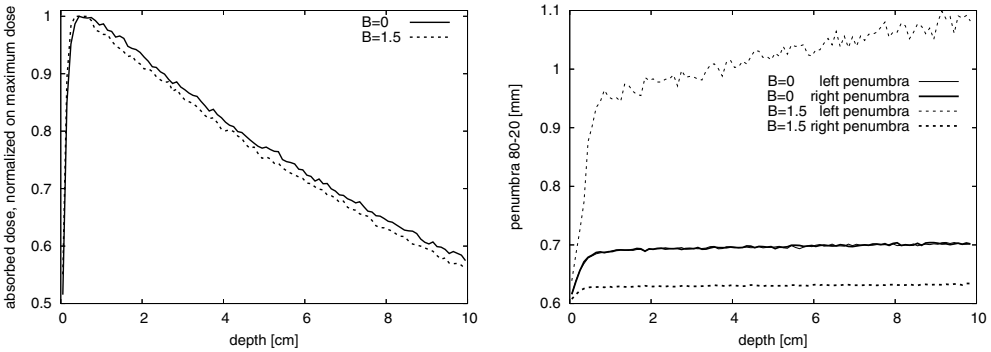

Figure 3. Monte Carlo simulations showing the central axis dose curve and the 80–20 penumbra for the pencil beam with and without the presence of 1.5 T. The solid lines show the 0 T case and the dashed lines the 1.5 T case. (a) Depth–dose curve. (b) 80–20 penumbra as a function of the depth. The penumbra on the left-hand side is in thin lines, the right-hand side in thick lines. The lines for the 0 T case are overlapping.

3. Results

3.1. Monte Carlo simulations of the dose deposition kernel in a 1.5 T field

In figure 3, the impact of the 1.5 T field on the pencil beam dose deposition kernel is shown. Figure 3(a) shows the dose–curve along the central axis of the pencil beam. One cannot speak of the build-up distance for a pencil beam since there is no lateral electron equilibrium. Still from figure 3(a) the difference due to the 1.5 T is quantified and found to be 3 mm. That is, it requires a 3 mm shift in the depth of the 1.5 T profile to match the part of the profile beyond maximum dose with the corresponding part of the 0 T case.

The main difference due to the magnetic field is expected as an asymmetry of the dose deposition in the lateral (X) direction. This is shown in figure 3(b) where the 80–20 penumbra in the X direction at both sides of the dose deposition is shown as a function of depth. After a few mm already a clear distinction between the situation with and without magnetic field is visible. Without the magnetic field, the penumbra is approximately 0.7 mm and (obviously) the penumbra at both sides of the dose deposition is equal (lines for left-hand side ($-X$ direction), and right-hand side ($+X$ direction) penumbra are overlapping). With a magnetic field present this is no longer true; the penumbra is either slightly smaller, 0.6 mm or larger, 1 mm.

3.2. Dose distributions of 1 × 1 and 5 × 5 cm^2 fields in the presence of a 1.5 T field

The pencil beam kernel as shown in section 3.1 is used to determine the dose distribution of 1×1 and $5 \times 5\,\mathrm{cm}^2$ fields in the presence of a 1.5 T field. Figure 4(a) shows the central dose profiles in the X direction at 5 cm depth. The asymmetry caused by the magnetic field can be seen clearly. The width at 50% for the $5 \times 5\,\mathrm{cm}^2$ field is unaffected by the magnetic field. However the entire field is shifted approximately 0.7 mm; this is true for all depths beyond maximum dose (not presented here) and this is also found for the $1 \times 1\,\mathrm{cm}^2$ field.

Figure 4(b) shows the impact on the depth–dose curve for the 1×1 and the $5 \times 5\,\mathrm{cm}^2$ field. The build-up distance decreases for the 1×1 and $5 \times 5\,\mathrm{cm}^2$ field with approximately 5 mm due to the 1.5 T magnetic field. This means a shift in the depth of 5 mm causes the

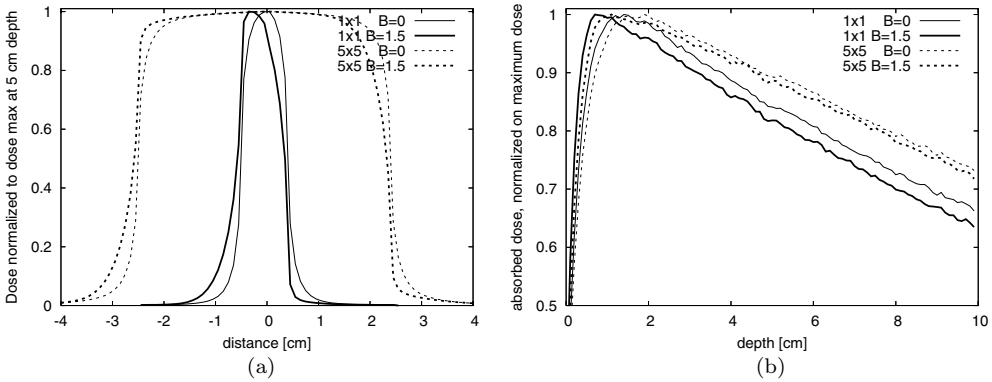

(a) (b)

Figure 4. Calculated central dose profiles in the X direction at 5 cm depth and the central axis depth–dose curves for 1×1 (solid lines) and $5 \times 5\,\mathrm{cm}^2$ fields (dashed lines). Both with (thick lines) and without (thin lines) the presence of 1.5 T. (a) Lateral dose profiles at 5 cm depth. (b) Depth–dose curves.

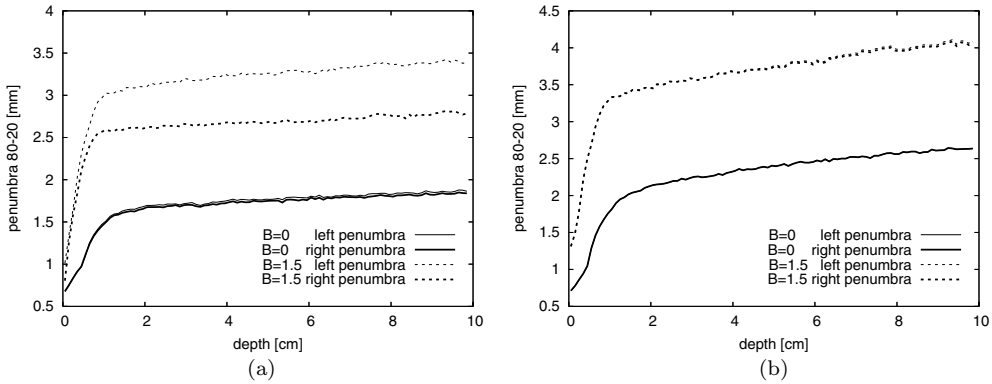

(a) (b)

Figure 5. The 80–20 penumbra as a function of the depth for both a 1×1 and a $5 \times 5\,\mathrm{cm}^2$ field with and without the presence of 1.5 T. The solid lines show the 0 T case and the dashed lines the 1.5 T case. The penumbra on the left-hand side is in thin lines, the right-hand side in thick lines. (a) $1 \times 1\,\mathrm{cm}^2$ field. The lines for the 0 T case are virtually overlapping. (b) $5 \times 5\,\mathrm{cm}^2$ field. Both the lines for the 0 and the 1.5 T case are overlapping.

profiles to coincide for the part beyond the maximum dose. While figure 4(a) shows very smooth graphs, figure 4(b) shows some noise due to the statistical nature of Monte Carlo modelling. This is because a pencil beam kernel is used in the convolution, the longitudinal direction, i.e. the resulting depth–dose curves, reflects this noise of the pencil beam kernel. In the plane perpendicular to the pencil beam, the convolution intrinsically blurs the noise, yielding smooth profiles as shown in figure 4(a).

In figure 5 the 80–20 penumbra of both fields is shown as a function of the depth. For both cases the penumbra increases by the presence of the magnetic field. For the $1 \times 1\,\mathrm{cm}^2$ field the lateral electron equilibrium is not fully reached anywhere in the field and the penumbra is asymmetric, although not as severe as for the pencil beam dose deposition. For the $5 \times 5\,\mathrm{cm}^2$ field, full lateral electron equilibrium exists in the central part of the field and the penumbra is perfectly symmetric, the lines for the left-hand side and the right-hand side penumbra are coinciding. Nevertheless the dose distribution is asymmetric as can be seen in figure 4(a). This will be discussed in section 4.1.

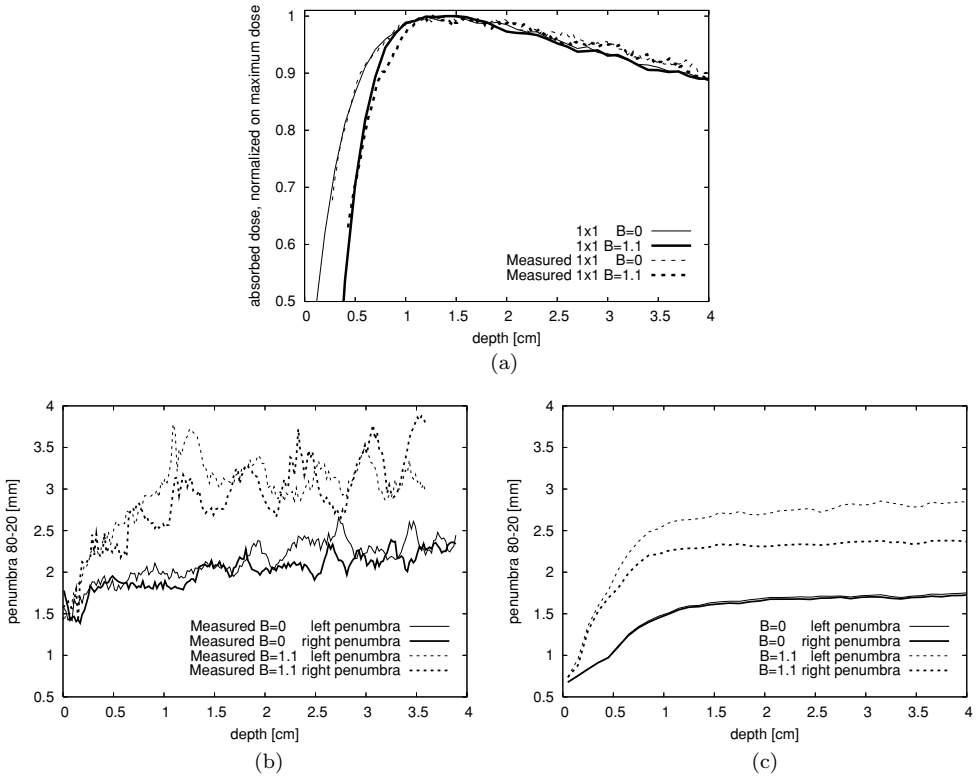

Figure 6. Film measurements and Monte Carlo simulations showing the depth–dose curve and the 80–20 penumbra for the $1 \times 1\,\mathrm{cm}^2$ field with and without the presence of 1.1 T. (a) Simulated (solid lines) and measured (dashed lines) depth–dose curves, both with (thick lines) and without (thin lines) 1.1 T. (b) Measured 80–20 penumbra as a function of the depth. The penumbra on the left-hand side is in thin lines, the right-hand side in thick lines. The solid lines show the 0 T case, the dashed lines the 1.1 T case. (c) Monte Carlo 80–20 penumbra as a function of the depth. The penumbra on the left-hand side is in thin lines, the right-hand side in thick lines. The solid lines show the 0 T case, the dashed lines the 1.1 T case.

3.3. Measured dose deposition of a 1 × 1 cm² field in the presence of a 1.1 T magnetic field

Figure 6 shows the measured and calculated depth–dose curves as well as the 80–20 penumbra as a function of depth for a $1 \times 1\,\mathrm{cm}^2$ field, both with and without the presence of 1.1 T. The measured depth–dose curve (figure 6(a)) is unreliable for very shallow depths (first few mm) whereas the maximum dose could be determined more precisely. Therefore the measurements and simulations, both with and without 1.1 T are plotted such that the part beyond maximum dose is coinciding. The required shift of the profiles is then a measure for the decrease in build up. For the simulations a shift (i.e. a decrease of build up) of 3 mm was found. For the measurements a shift between 2 and 3 mm was found.

The 80–20 penumbra, as presented in figures 6(b) and 6(c), clearly increases in the presence of the magnetic field. Both the measurements and the simulations show an increase for the 80–20 penumbra of approximately 1 mm. The asymmetry between left-hand and right-hand side penumbra as visible in figure 6(c) cannot be judged from the measurements in figure 6(b).

For the simulations a shift of approximately 0.4–0.5 mm of the 50% isodose line was found (not presented here), this measure could not be determined for the experimental set-up because the films were not positioned according to the beam axis in an absolute way.

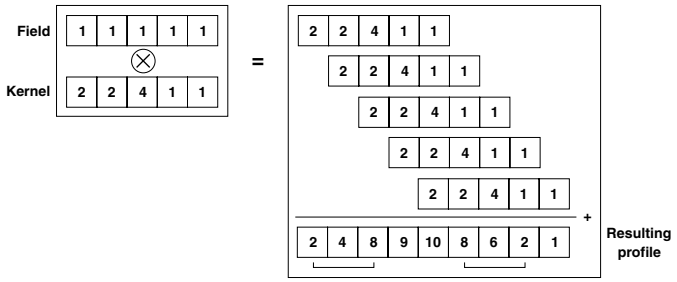

Figure 7. Schematic illustration of convolving a pencil beam kernel with a given field in one-dimension. The maximum reached in the convolution is the sum of all kernel values: 10. The profile is clearly asymmetric but the 80–20 penumbra, as indicated by the horizontal brackets, is perfectly symmetric, namely 2 'voxels'.

4. Discussion

4.1. Dose deposition in 1.5 T

The pencil beam dose deposition kernel is clearly asymmetric in the direction perpendicular to the 1.5 T magnetic field, as seen in figure 3. For larger fields the asymmetry induced by the magnetic field decreases, as shown for the $1 \times 1\,\mathrm{cm}^2$ field in figures 4(a) and 5(a). As soon as lateral electron equilibrium in the central part of the field exists, as is the case for the $5 \times 5\,\mathrm{cm}^2$ field, the asymmetry in the penumbra disappears (figure 5(b)), whereas the dose distribution remains asymmetric as can be seen in figure 4(a). For this case the penumbra increases approximately 1 mm by the presence of 1.5 T.

It seems counter intuitive that the 80–20 penumbra becomes symmetric whereas a dose profile is clearly asymmetric. Still this is straightforward with the convolution method in mind. Basically, taking the convolution is placing a number of pencil beam kernels side to side, filling up the required field size, given a certain normalization and a finite kernel size. Figure 7 shows a diagram in which this is illustrated for an example in one-dimension. The left-hand slope is determined by the integral of the kernel. The maximum is determined by the integration of the entire kernel along the given profile. The right-hand slope is determined according to the same integral, only starting at the other side. This yields the same, albeit mirrored, slope and therefore the 80–20 penumbra, as this is a relative measure within this slope, will be the same for both sides. Note that the maximum is only reached if the profile is wide enough to integrate all values of the kernel for this profile, i.e. for our situation, that there is a lateral electron equilibrium.

Despite the asymmetric dose deposition the abutment of fields is not affected. Adding a number of pencil beam kernels (i.e. taking the convolution) to obtain a $5 \times 5\,\mathrm{cm}^2$ field does yield a flat field as shown in figure 4(a).

Besides the increased penumbra, the 1.5 T magnetic field causes a shift of approximately 0.7 mm of the 50% isodose line. Also the impact on the build-up distance becomes noticeable. The latter decreases by approximately 5 mm, as seen in figure 4.

4.2. Dose deposition in 1.1 T

The measurements were limited to a $1 \times 1\,\mathrm{cm}^2$ field and to 1.1 T magnetic field. As mentioned in section 2.1 the Monte Carlo simulations are neglecting various elements of the measurements; however, they do use the correct photon energy spectrum. The effect of the magnetic field is

determined by the energy of the (secondary) electrons, so by the photon energy spectrum and the magnetic field strength. These are the two quantities that are taken into account correctly and therefore the magnitude of the impact of the magnetic field can be compared between measurements and simulations. They are shown to be in agreement.

The behaviour of the dose deposition in 1.1 T is very similar to that in 1.5 T. The difference is that the increase in penumbra and the shift of the 50% isodose line are both slightly smaller, the difference between the depth–dose curves of 1.1 and 1.5 T is too small to be evaluated.

5. Conclusion

For this specific configuration, the magnitude of the impact of the magnetic field as measured in 1.1 T was found to be in agreement with the corresponding Monte Carlo simulations.

For radiation fields where the lateral electron equilibrium exists, the impact of the 1.5 T magnetic field on the dose deposition by a 6 MV photon beam can be summarized as follows: a decrease of the build-up distance by 5 mm, a symmetric increase in the penumbra in the direction perpendicular to the magnetic field by 1 mm and in the same direction a shift of the entire radiation field by approximately 0.7 mm. For fields too small to have lateral electron equilibrium in the central part of the field, the penumbra in the direction perpendicular to the magnetic field becomes asymmetric.

Abutting radiation fields in the presence of a magnetic field does not yield problems. For treatment planning, the increased penumbra and reduced build-up distance can be incorporated in a conventional manner. The induced 0.7 mm shift of the isodose line in the direction perpendicular to the magnetic field requires the inclusion of asymmetric and direction-dependent dose profiles.

In conclusion, the impact on the dose deposition for our specific configuration of a 6 MV photon beam in a transverse 1.5 T magnetic field can be taken into account in a conventional treatment planning procedure, with special attention being paid to the direction-dependent dose shift of 0.7 mm.

For single fields, the overall impact of the magnetic field is small. For instance the shift of 0.7 mm can easily be dismissed. However for IMRT treatments, when abutting segments from different gantry positions, under- or over-dosage can occur. The impact of the altered dose deposition for clinical IMRT treatments is the topic of further research.

Acknowledgment

The authors wish to thank Wiebe van der Zee for his help on the photon beam energy spectrum as used in the Monte Carlo simulations.

References

Agostinelli S *et al* 2003 Geant4—a simulation toolkit *Nucl. Instrum. Methods Phys. Res.* A **506** 250–303

Bielajew A F 1993 The effect of strong longitudinal magnetic fields on dose deposition from electron and photon beams *Med. Phys.* **20** 1171–9

Briesmeister J F 1997 MCNP: a general Monte Carlo *N*-particle transport code-version 4b *Tech. Rep. LA-12625* Los Alamos National Laboratories, Los Alamos, NM

Carrier J F, Archambault L and Beaulieu L 2004 Validation of Geant4, an object-oriented Monte Carlo toolkit, for simulations in medical physics *Med. Phys.* **31** 484–92

Drake D G, Jaffray D A and Wong J W 2000 Characterization of a fluoroscopic imaging system for kv and mv radiography *Med. Phys.* **27** 898–905

Gilhuijs K G A, Van de Ven P J H and Van Herk M 1996 Automatic three-dimensional inspection of patient setup in radiation therapy using portal images, simulator images, and computed tomography data *Med. Phys.* **23** 389–99

Groh B A, Siewerdsen J H, Drake D G, Wong J W and Jaffray D A 2002 A performance comparison of flat-panel imager-based MV and kV cone-beam CT *Med. Phys.* **29** 967–75

International Commission on Radiation Units and Measurements (ICRU) 1999 Prescribing, recording and reporting photon beam therapy *ICRU Report* No. 62 (Bethesda, MD: ICRU)

Jaffray D A, Siewerdsen J H, Wong J W and Martinez A A 2002 Flat-panel cone-beam computed tomography for image-guided radiation therapy *Int. J. Radiat. Oncol. Biol. Phys.* **53** 1337–49

Jette D 2000a Magnetic fields with photon beams: dose calculation using electron multiple-scattering theory *Med. Phys.* **27** 1705–16

Jette D 2000b Magnetic fields with photon beams: Monte carlo calculations for a model magnetic field *Med. Phys.* **27** 2726–38

Khan F M 1994 *The Physics of Radiation Therapy* 2nd edn (Baltimore, MD: Williams & Wilkins)

Kawrakow I 2000 Accurate condensed history Monte Carlo simulation of electron transport: I. EGSnrc, the new EGS4 version *Med. Phys.* **27** 485–98

Lagendijk J J W, Raaymakers B W, Van Der Heide U A, Topolnjak R, Dehnad H, Hofman P, Nederveen A J, Schulz I M, Welleweerd J and Bakker C J G 2002 MRI guided radiotherapy: MRI as position verification system for IMRT *Radiother. Oncol.* **64** (Suppl 1) 224 (Czech Republic European Society for Therapeutic Radiation Oncology)

Ling C C, Humm J, Larson S, Amols H, Fuks Z, Leibel S and Koutcher J A 2000 Towards multidimensional radiotherapy (MD-CRT): biological imaging and biological conformality *Int. J. Radiat. Oncol., Biol. Phys.* **47** 551–60

Litzenberg D W, Fraass B A, McShan D L, O'Donnel T W, Roberts D A, Becchetti F D, Bielajew A F and Moran J M 2001 An apparatus for applying strong longitudinal magnetic fields to clinical photon and electron beams *Phys. Med. Biol.* **46** N105–15

Mackie T R, Holmes T, Swerdloff S, Reckwerdt P, Deasy J O, Yang J, Paliwal B and Kinsella T 1993 Tomotherapy: a new concept for the delivery of dynamic conformal radiotherapy *Med. Phys.* **20** 1709–19

Nardi E and Barnea G 1999 Electron beam therapy with transverse magnetic fields *Med. Phys.* **26** 967–73

Nederveen A J, Lagendijk J J W and Hofman P 2001 Feasibility of automatic marker detection with an a-Si flat-panel imager *Phys. Med. Biol.* **46** 1219–30

Nelson W R, Hirayama H and Rogers D W O 1985 The EGS4 code system *Stanford Linear Accelerator Center Report 265* Stanford University Stanford, CA, USA

Raaymakers B W, Lagendijk J J W, Van der Heide U A, Overweg J, Brown K, Topolnjak R, Dehnad H, Jurgenliemk-Schulz I M, Welleweerd J and Bakker C J G 2004 Integrating an MRI scanner with a radiotherapy accelerator: a new concept of precise on line radiotherapy guidance and treatment monitoring *Proc. 14 Int. Conf. on the Use of the Computers in Radiation Therapy (Seoul, South Korea)*

Reiffel L, Li A, Chu J, Wheatley R W, Naqvi S, Pillsbury R and Saxena A 2000 Control of photon beam dose profiles by localized transverse magnetic fields *Phys. Med. Biol.* **45** N177–82

Rogers D W O, Faddegon B A, Ding G X, Ma C M, We J and Mackie T R 1995 Beam: a Monte Carlo code to simulate radiotherapy treatment units *Med. Phys.* **22** 503–24

Ruchala K J, Olivera G H, Schloesser E A and Mackie T R 1999 Megavoltage ct on a tomotherapy system *Phys. Med. Biol.* **44** 2597–621

Serago C H, Chungbin S J, Buskirk S J, Ezzeli G A, Collie A C and Vora S A 2002 Initial experience with ultrasound localization for positioning prostate cancer patients for external beam radiotherapy *Int. J. Radiat. Oncol. Biol. Phys.* **53** 1130–8

Shirato H *et al* 2000 Four-dimensional treatment planning and fluoroscopic real-time tumor tracking radiotherapy for moving tumor *Int. J. Radiat. Oncol. Biol. Phys.* **48** 435–42

Stroom J C and Heijmen B J M 2002 Geometrical uncertainties, radiotherapy planning margins, and the ICRU-62 report *Radiother. Oncol.* **64** 75–83

Suchowerska N, Hoban P, Butson M, Davison A and Metcalfe P 2001 Directional dependence in film dosimetry: radiographic and radiochromic film *Phys. Med. Biol.* **46** 1391–7

Van der Zee W and Welleweerd J 1999 Calculating photon beam characteristics with Monte Carlo techniques *Med. Phys.* **26** 1883–92

Van Herk M, Remeijer P, Rasch C and Lebesque J V 2000 The probability of correct target dosage: dose-population histograms for deriving treatment margins in radiotherapy *Int. J. Radiat. Oncol., Biol. Phys.* **47** 1121–35